



This is a repository copy of *Concurrent, Tunable, Multi-band, Single Chain Radio Receivers for 5G RANs* .

White Rose Research Online URL for this paper:
<http://eprints.whiterose.ac.uk/118287/>

Version: Accepted Version

Proceedings Paper:

Singh, R., Bai, Q., O'Farrell, T. orcid.org/0000-0002-7870-4097 et al. (2 more authors) (2017) *Concurrent, Tunable, Multi-band, Single Chain Radio Receivers for 5G RANs*. In: *2017 IEEE 85th Vehicular Technology Conference (VTC Spring)*. 2017 IEEE 85th Vehicular Technology Conference, 04-07 Jun 2017, Sydney, Australia. IEEE . ISBN 978-1-5090-5932-4

<https://doi.org/10.1109/VTCSpring.2017.8108423>

Reuse

Unless indicated otherwise, fulltext items are protected by copyright with all rights reserved. The copyright exception in section 29 of the Copyright, Designs and Patents Act 1988 allows the making of a single copy solely for the purpose of non-commercial research or private study within the limits of fair dealing. The publisher or other rights-holder may allow further reproduction and re-use of this version - refer to the White Rose Research Online record for this item. Where records identify the publisher as the copyright holder, users can verify any specific terms of use on the publisher's website.

Takedown

If you consider content in White Rose Research Online to be in breach of UK law, please notify us by emailing eprints@whiterose.ac.uk including the URL of the record and the reason for the withdrawal request.



eprints@whiterose.ac.uk
<https://eprints.whiterose.ac.uk/>

Concurrent, Tunable, Multi-band, Single Chain Radio Receivers for 5G RANs

R. Singh, *Member, IEEE*, Q. Bai, T. O'Farrell, *Member, IEEE*, K. L. Ford, *Senior Member, IEEE*, and R. J. Langley, *Senior Member, IEEE*

Abstract—A concurrent, tunable, tri-band, single chain radio receiver for 5G radio access networks is evaluated. The three concurrent bands are independently tunable over a frequency range from 600 MHz to 2.7 GHz. A hardware-in-the-loop test-bed provides a system level evaluation of the proposed receiver using direct RF digitization. The test-bed emulates a 5G heterogeneous network supporting three wideband, simultaneous connections. By measuring the receiver EVM, we demonstrate sufficient isolation between concurrent bands achieving 60 MHz of aggregated bandwidth as well as strong resilience to adjacent blockers.

Index Terms—Multi-band Systems, Reconfigurable Architectures, System Analysis and Design, Digital Radio Receivers, Heterogeneous Networks

I. INTRODUCTION

The fifth generation (5G) of cellular mobile radio access technologies (RATs) is expected to be highly heterogeneous operating with ultra dense radio access networks (RANs) consisting of legacy and new RATs to support the ever growing demand for high data transmission rates, lower latencies and higher energy efficiencies [1][2][3]. This will require the user equipment (UE) and the base transceiver stations (BTSs) to incorporate multiple radio units, each for a different RAT, which will increase the total number of radio transceiver chains at both ends of the wireless link. This would substantially increase the size, power consumption, complexity and cost of the radio equipment in a 5G RAN [4].

Additionally, this RF bottleneck could potentially restrict the usability of a UE to one geographic region, which only allows use of specific frequency bands. Therefore, in order to meet the expectations of the 5G RAN in a compact and power efficient manner, there is a need for the development of single transceiver chain, concurrent multi-band (CM), frequency-agile radio (FARAD) units, which can enable multiple, concurrent, frequency-agile data links between the BTSs and UE. Such radio units will allow the available spectrum at any geographical location to be efficiently aggregated through concurrent bands to achieve higher data transmission rates and quality of service via an always connected capability.

Direct RF digitisation can lead to frequency-agile, reconfigurable and power efficient radio front-ends [5], which have the CM transmission ability through a single transceiver chain [6]. We have recently proposed the design of a sub 1 GHz, concurrent, dual-band, frequency-agile radio receiver and tested the receiver through a hardware-in-the-loop test-bed [6]. In this paper, we present and characterise a novel concurrent triple-band single chain radio receiver, increasing

the number of concurrent bands to three and extending the RF transmission capability from 0.6 GHz to 2.7 GHz.

The triple-band radio receiver hardware-in-the-loop test-bed utilises a tunable triple-band antenna, a digital oscilloscope, a reconfigurable triple-channel digital down converter (DDC) and baseband processing unit. The receiver is characterised based on a potential 5G RAN scenario, where a single chain CM UE receives three independent data streams from three different BTSs. The receive signal quality of each data link is evaluated through error vector magnitude (EVM) measurements. In order to investigate potential interference between the bands the EVM measurements are carried out both in concurrent (all bands enabled) and individual (only one band enabled at a time) data transmission modes. The results show that there is no significant inter-band interference (IBI) between the concurrent transmissions and up to 60 MHz of aggregate transmission bandwidth can be achieved.

Further, an investigation into in-band co-located and adjacent channel interference is made through the use of artificial wideband single-carrier (SC) modulated blocker signals transmitted over adjacent/co-located channels to the wanted signals. The results show that the adjacent blocker signals do not affect the transmission quality of the wanted signals as long as their relative power is no more than ~ 10 dB of that of the wanted signals. The results also show that through the use of a small guard band between the wanted and adjacent blocker signals, the receiver's EVM performance is not affected by a blocker signal with up to 30 dB higher power relative to the wanted signals.

II. SYSTEM DESCRIPTION

This section provides a description of the test-bed at both the transmitter (Tx) and receiver (Rx) ends used for the characterisation of the triple-band, single chain receiver utilising the sub 3 GHz LTE bands.

A. Transmitter

A system level block diagram of the test-bed is shown in Fig. 1 (left). At the heart of the hardware-in-the-loop test-bed is the controller (PXIe-8135) [7], which is essentially a PC running LabVIEW and MATLAB software packages. The baseband signal processing takes place in the controller, where three independent baseband I/Q signals are generated in LabVIEW and sent to the dedicated reconfigurable RF signal generators (PXIe-5791/5793) [8][9] operating at three distinct RF frequencies. The RF output of the signal generators

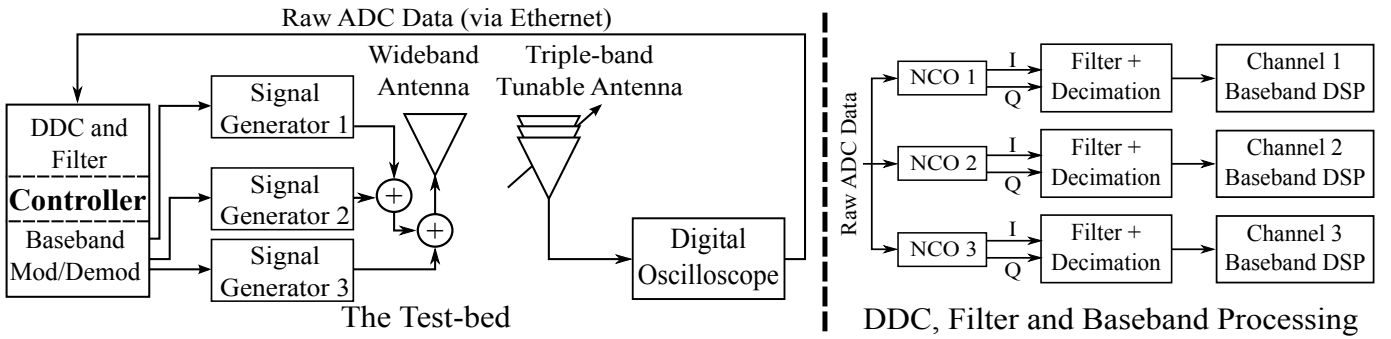


Fig. 1. Schematic of the direct RF digitising tri-band test-bed, DDC, decimation filter and baseband processing.

is combined (ZAPD-2-272-S+) [10] and transmitted using a wideband antenna (UHALP-9108 A) [11].

B. Receiver

The RF digitising, single chain receiver comprises a tunable triple-band antenna, a digital storage oscilloscope (DSO) [12] acting as an RF digitiser, a reconfigurable triple-channel digital down-converter (DDC) and baseband processors.

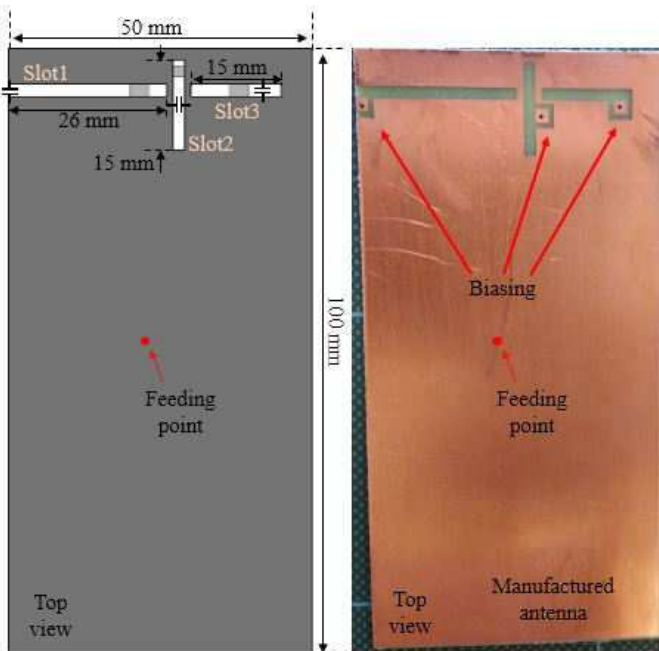


Fig. 2. Tunable tri-band antenna structure

Tunable Tri-band Antenna: The antenna used in the receiver is an independently tunable tri-band slot antenna, which was developed from the previous tunable dual-band antenna prototype presented in [13]. The antenna is manufactured on a 50×100 mm FR4 printed circuit board (PCB), and is able to provide three concurrent and independently tunable frequency bands operating over the frequency range from 600 MHz to 2.7 GHz.

As shown in Fig. 2, the antenna has three tunable slots located near the top edge of the PCB, which are used as the basic radiation elements to achieve three tunable frequency

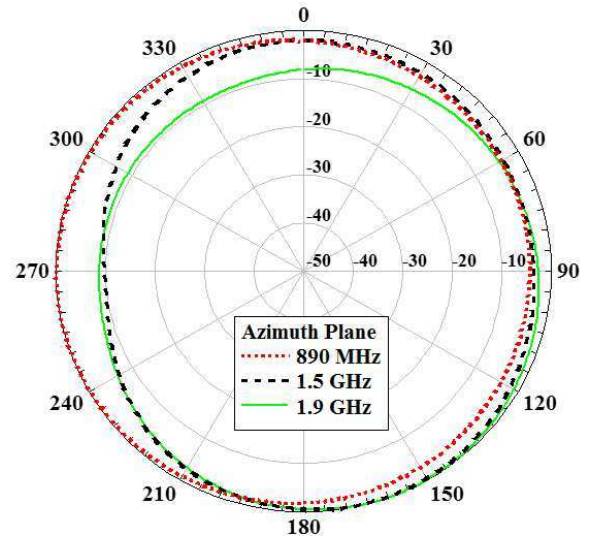


Fig. 3. Antenna azimuth radiation patterns at 890 MHz, 1.5 GHz and 1.9 GHz

bands. Due to the limited frequency tuning range of a single slot, the total desired frequency ranges are divided into three sub-ranges: 0.6 to 1.1 GHz, 1 to 2.5 GHz and 1.9 to 2.7 GHz, which are covered by slots 1, 2 and 3 in Fig. 2, respectively. Each slot provides 30 MHz, 100 MHz and 40 MHz operating bandwidth at the test-bed frequencies 890 MHz, 1.5 GHz and 1.9 GHz, respectively. The antenna azimuth radiation patterns at these three targeted frequencies are plotted in Fig. 3.

Digital Down-Conversion and Baseband DSP: The mixed RF signal detected by the triple-band antenna is directly digitised by the DSO at a sampling rate of 10 GSps in the receiver chain. The controller acquires the digitised signal (or the raw ADC samples) from the DSO through a direct Ethernet link, before performing DDC and baseband demodulation.

The block diagram of a triple-channel DDC is shown in Fig. 1 (right) together with the baseband processing units. DDC provides frequency conversion and decimation filtering of the desired bands before the baseband demodulation takes place. The real digital RF signal in the form of ADC samples is mixed with complex outputs of three different digital synthesisers known as numerically controllable oscillators (NCO). The DDC was implemented as a direct (or homodyne) converter. Therefore, the centre frequencies of the NCOs were

set equal to the carrier frequencies of the signals generated at the Tx. This provides the baseband I/Q samples for the three concurrent channels at the receiver.

The baseband signals then pass through the cascaded integrated comb (CIC) decimation filters, which provide image and out-of-band rejection, as well as sample rate reduction to a desired level. In this work, the DDC was implemented using a MATLAB DSP function, where the NCO centre frequencies, the CIC stopband frequencies and attenuation, and the decimation factors were configured according to the bandwidths and carrier frequencies of the incoming signals. The filtered, decimated baseband signals are then processed in LabVIEW, where the timing, carrier and phase offsets are removed through the use of a synchronisation sequence and by locking to the carrier signal. Then matched filtering is performed before the *rms* EVM is estimated through equation (1) [14], where N is the number of samples received, I and Q are the ideal in-phase and quadrature levels, and \tilde{I} and \tilde{Q} are the received in-phase and quadrature values.

$$\text{EVM}_{rms} = \sqrt{\frac{\frac{1}{N} \sum_{i=1}^N (I_i - \tilde{I}_i)^2 + (Q_i - \tilde{Q}_i)^2}{\frac{1}{N} \sum_{i=1}^N (I_i^2 + Q_i^2)}} \quad (1)$$

III. SYSTEM LEVEL PERFORMANCE IN A HETNET SCENARIO

We consider a 5G HetNet scenario which can concurrently connect a user to a macro-cell BTS at 890 MHz and to two small-cell BTSs at 1500 and 1900 MHz. The CM receiver aims to maintain similar transmission quality across corresponding radio links when operating in concurrent or independent transmission modes.

Three independent QPSK single-carrier (SC) signals, centered at 890 MHz, 1500 MHz and 1900 MHz, were transmitted at the same power. Signal bandwidths of 10 and 20 MHz were considered for each transmission, yielding total system bandwidths of 30 and 60 MHz, respectively. Fig. 4 (a) & (b) show the EVM vs. received SNR for the three processed signals in concurrent transmission mode for 10 and 20 MHz bandwidths, respectively. While the performance of the three bands are more or less equivalent, there is an SNR penalty in the 20 MHz band *cf.* the 10 MHz band. The EVM performances for the same QPSK SC signals were measured separately and the results are plotted in Fig. 5 (a) & (b). The curves for separately measured channels are almost identical to those for the concurrent case. This can also be confirmed from Fig. 6 & Fig. 7, where the EVM results are plotted over the received power (dBm).

We also considered unwanted blocker signals, which may appear at adjacent frequencies to the wanted signals [15] [16]. In general, blockers are attenuated at the front-end by the filtering characteristics of our tunable antenna. However, as the bandwidths of each band change at different tuning frequencies, the adjacent blockers may interfere unless additional digital filtering is considered. The EVM performance of each band was evaluated in the presence of a QPSK SC blocker located adjacent to or co-located with the wanted bands. The

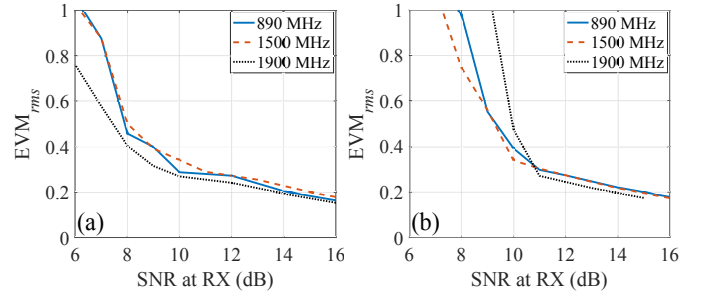


Fig. 4. EVM_{rms} performance of *concurrent multi-band* QPSK modulated single-carrier transmissions over the tri-band test-bed, a) A 10 MHz wide transmission and b) a 20 MHz wide transmission.

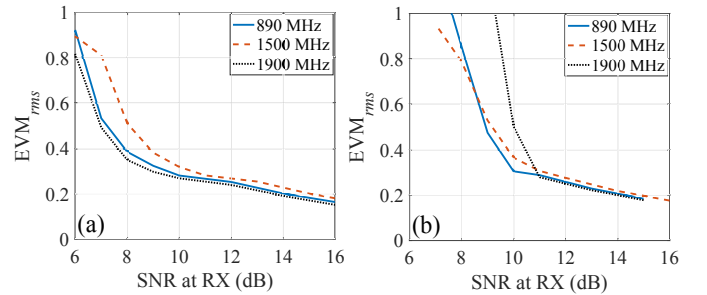


Fig. 5. EVM_{rms} performance of *independent* QPSK modulated single-carrier transmissions over the tri-band test-bed, a) A 10 MHz wide transmission and b) a 20 MHz wide transmission.

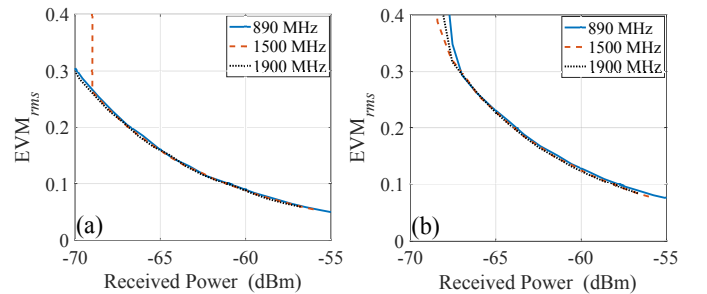


Fig. 6. EVM_{rms} performance of *concurrent multi-band* QPSK modulated single-carrier transmissions over the tri-band test-bed, a) A 10 MHz wide transmission and b) a 20 MHz wide transmission.

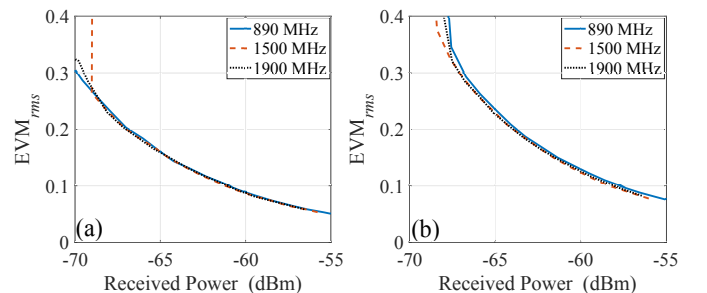


Fig. 7. EVM_{rms} performance of *independent* QPSK modulated single-carrier transmissions over the tri-band test-bed, a) A 10 MHz wide transmission and b) a 20 MHz wide transmission.

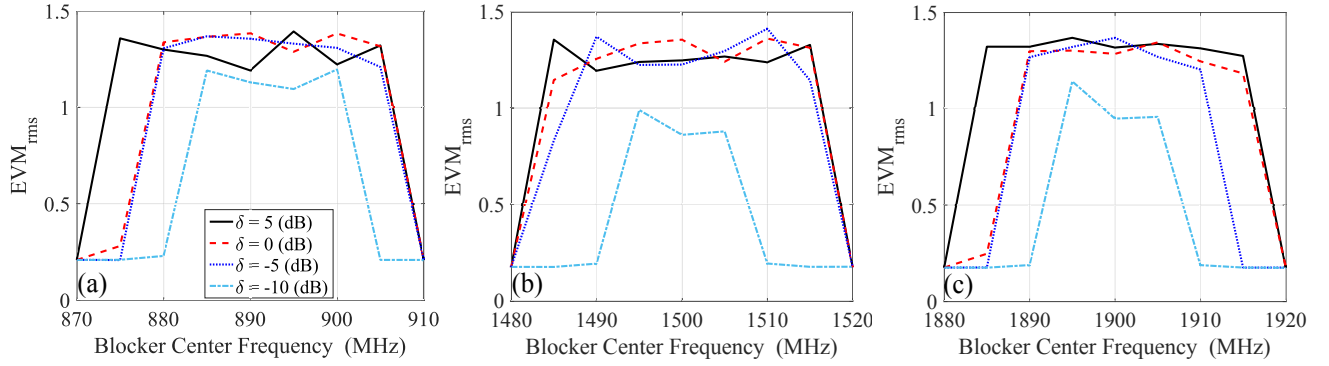


Fig. 8. The effect of 20 MHz wide adjacent/co-located SC blockers on the EVM performance of 20 MHz wide concurrent single-carrier transmissions at a) 890 MHz, b) 1.5 GHz and c) 1.9 GHz.

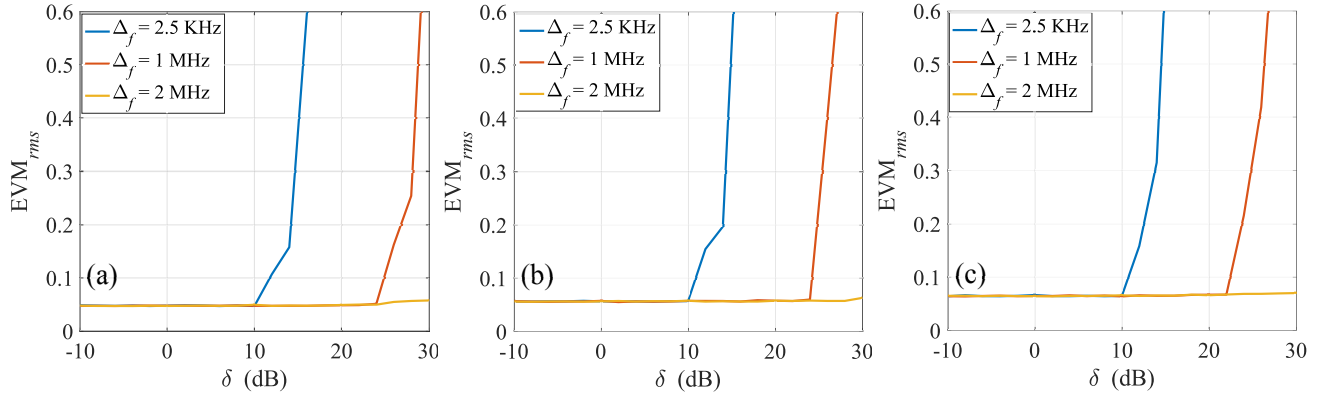


Fig. 9. The effect of 10 MHz wide adjacent SC blockers on the EVM performance of 10 MHz wide concurrent single-carrier transmissions at a) 890 MHz, b) 1500 MHz and c) 1900 MHz.

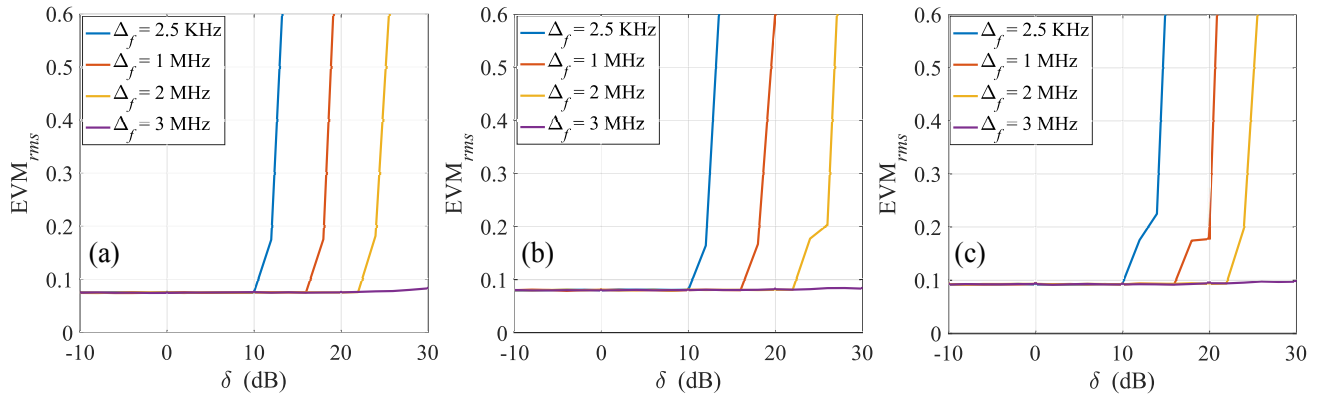


Fig. 10. The effect of 20 MHz wide adjacent SC blockers on the EVM performance of 20 MHz wide concurrent single-carrier transmissions at a) 890 MHz, b) 1500 MHz and c) 1900 MHz.

power of the blocker signal was varied such that the ratio of the received power of the blocker relative to the received power of the wanted signals, denoted δ , changed from -10 to +30 dB. The blocker signal was generated and transmitted by a separate signal generator (SMBV100A) and wide-band antenna (UHALP-9108 A), respectively.

We first evaluated the EVM performance of the concurrently transmitted wanted signals in the presence of co-located blocker signals for a bandwidth of 20 MHz. The results are presented in Fig. 8, which shows that the EVM of each

transmission is severely affected by a blocker signal which is fully co-located or has a spectral overlap with the wanted signals. The results in Fig. 8 also show that the EVM of the wanted signals is not affected by the adjacent blocker for a δ of -10 to +5 dB, provided the blocker signal was centered 20 MHz or more away from the wanted signal, thereby avoiding spectral overlap. Some spectral overlap can be tolerated for low power blocker signals. The results in Fig. 8 show that the QPSK SC blockers produced an EVM greater than unity when the center frequencies of the blocker and wanted signals were

co-located.

To further study the effect of adjacent blocker signals with larger δ values, we evaluated the EVM performance of the 10 and 20 MHz wide concurrent transmission in the presence of adjacent blockers with δ of up to 30 dB. The results for this investigation are shown in Fig. 9 and Fig. 10 for the 10 and 20 MHz bandwidth, respectively. These results show that none of the adjacent blocker signals will interfere with the wanted signals for up to a δ of approximately 10 dB. However, as the δ is further increased, the EVM performance of the wanted signals will degrade from ~ 0.1 to be greater than ~ 0.6 if no guard band (Δ_f) is used. Therefore, use of a guard band becomes important to avoid interference from adjacent channels. The results show that for δ of up to 30 dB a Δ_f of 2 and 3 MHz each side of the 10 and 20 MHz wide wanted signal, respectively, will be sufficient to avoid any significant ACI from a wideband blocker in our test-bed. These results show that the receiver is able to match standard specific ACI performance with a guard band, given the LTE release 12 also specifies that the receiver must be resilient to adjacent blocker signals with a δ of up to 25.5 dB [17].

IV. CONCLUSIONS AND FUTURE WORK

Overall the results show that the combined antenna and digital CIC filtering effectively prevent interband interference whilst rejecting interference from adjacent wideband blocker signals with up to 30 dB higher relative power. However, the results also show that a partially or fully co-located blocker increases the EVM of the wanted signals from ~ 0.1 to ~ 1.3 . Increasing the receiver tunable range up to 6 GHz is a topic of future research by the authors.

V. ACKNOWLEDGEMENT

This work was carried out in the FARAD project funded by the UK government under the EPSRC grant EP/M013723/1. The work is also supported by the UK Mobile Virtual Centre of Excellence.

REFERENCES

[1] NGMN Alliance, "5G white paper," *Next Generation Mobile Networks, White paper*, 2015.

- [2] J. He, P. Loskot, T. O'Farrell, V. Friderikos, S. Armour, and J. Thompson, "Energy efficient architectures and techniques for green radio access networks," in *Communications and Networking in China (CHINACOM), 2010 5th International ICST Conference on*. IEEE, 2010, pp. 1–6.
- [3] H. Hamdoun, P. Loskot, T. O'Farrell, and J. He, "Survey and applications of standardized energy metrics to mobile networks," *Annals of telecommunications-Annales des télécommunications*, vol. 67, no. 3–4, pp. 113–123, 2012.
- [4] W. Guo and T. O'Farrell, "Green cellular network: Deployment solutions, sensitivity and tradeoffs," in *Wireless Advanced (WiAd), 2011*. IEEE, 2011, pp. 42–47.
- [5] Texas Instruments, "RF Sampling and GSPS ADCs: Breakthrough ADCs Revolutionize Radio Architectures," 2012. [Online]. Available: <http://www.ti.com/lit/sg/snwt001/snwt001.pdf>
- [6] R. Singh, Q. Bai, T. O'Farrell, K. L. Ford, and R. J. Langley, "Demonstration of RF Digitising Concurrent Dual-Band Receiver for Carrier Aggregation over TV White Spaces," in *84th Vehicular Technology Conference (VTC2016-Fall), 2016 IEEE, Accepted for Publication, Sep 2016*.
- [7] National Instruments, "Embedded Controller, PXIe-8135." [Online]. Available: <http://www.ni.com/datasheet/pdf/en/ds-403>
- [8] —, "Embedded Signal Generator, PXIe-5793." [Online]. Available: <http://www.ni.com/pdf/manuals/373949b.pdf>
- [9] —, "Embedded Signal Transceiver, PXIe-5791." [Online]. Available: <http://www.ni.com/pdf/manuals/373845d.pdf>
- [10] Mini Circuits, "Power Combiner/Splitter, ZAPD-2-272-S+." [Online]. Available: <http://194.75.38.69/pdfs/ZAPD-2-272+.pdf>
- [11] Schwarzbeck, "Log-Periodic Antenna, UHALP-9108 A." [Online]. Available: <http://www.schwarzbeck.de/en/antennas/logarithmic-periodic-broadband-antennas/standard-lpda/205-uhalp-9108-a.html>
- [12] LeCroy, "WaveSurfer MXs-A Oscilloscopes 200 MHz 1 GHz, 104MXs-A." [Online]. Available: <http://teledynelecroy.com/japan/pdf/cata/wsxs-msxs-a-ds-12oct10-pdf.pdf>
- [13] Q. Bai, R. Singh, K. L. Ford, R. J. Langley, and T. O'Farrell, "Tunable Dual-band Antenna for Sub GHz Cellular Mobile Radio Applications," in *Loughborough Antennas and Propagation Conference (LAPC), 2016 IEEE, Accepted for Publication, Nov 2016*.
- [14] "IEEE Standard for Local and Metropolitan Area Networks Part 16: Air Interface for Fixed Broadband Wireless Access Systems," *IEEE Std 802.16-2004 (Revision of IEEE Std 802.16-2001)*, pp. 01–857, 2004.
- [15] L. Aguado, K. Wong, and T. O'Farrell, "Coexistence issues for 2.4 GHz OFDM WLANs," in *3G Mobile Communication Technologies, 2002. Third International Conference on (Conf. Publ. No. 489)*. IET, 2002, pp. 400–404.
- [16] K. Wong and T. O'Farrell, "Coverage of 802.11 g WLANs in the presence of Bluetooth interference," in *Personal, Indoor and Mobile Radio Communications, 2003. PIMRC 2003. 14th IEEE Proceedings on*, vol. 3. IEEE, 2003, pp. 2027–2031.
- [17] Evolved Universal Terrestrial Radio Access, "LTE; Evolved Universal Terrestrial Radio Access (E-UTRA); User Equipment (UE) conformance specification; Radio transmission and reception; Part 1: Conformance testing (3GPP TS 36.521-1 version 12.3.0 Release 12)," 2014.